Research Square

Preprints are preliminary reports that have not undergone peer review.
They should not be considered conclusive, used to inform clinical practice,
or referenced by the media as validated information.

Collective Modes in Neural Nets and their Dissipative Dynamics

Graziano Terenzi
Oxhy Labs, Oxhy Srl.
Giuseppe Vitiello
givitiello@unisa.it

University of Salerno

Research Article

Keywords: Mesoscopic neurodynamics, Dissipative neural fields, Spontaneous symmetry breaking, Long-range correlations, Collective modes

Posted Date: November 6th, 2026

DOI: https://doi.org/10.21203/rs.3.rs-11235158/v1

License: This work is licensed under a Creative Commons Attribution 4.0 International License.
Read Full License

Additional Declarations: No competing interests reported.

Collective Modes in Neural Nets and their Dissipative Dynamics

Graziano Terenzi[1] and Giuseppe Vitiello[2*†]

[1]Oxhy Labs, Oxhy Srl, Via Coroglio 57, Napoli, 80124, Italy.
[2*]Department of Physics "E.R. Caianiello", University of Salerno, Via Giovanni Paolo II 132, Fisciano, 84084, (Salerno), Italy.

*Corresponding author(s). E-mail(s): givitiello@unisa.it;
Contributing authors: graziano.terenzi@gmail.com;
†These authors contributed equally to this work.

Abstract

Walter Freeman's mesoscopic neurodynamics placed a fundamental problem at the center of brain science, i.e. how local neural activity gives rise to coherent organization at the scale of whole populations. Here we explore this problem by means of a finite dissipative neural field model. Starting from an initially unbiased lattice of interacting complex SU(2) doublets, a transient external input drives the network toward a stable macroscopic order. After the input is removed, the neural field continues to reorganize spontaneously around the established order, while coordinated fluctuations and spatial patterns emerge across distant regions of the lattice. These features provide finite-size signatures of the same organizing principles that, in Quantum Field Theory, are associated with spontaneous symmetry breaking and collective modes. Importantly, they appear in a finite system, without requiring the thermodynamic limit. Such finite neural fields therefore offer not only a bridge between local dynamics and collective organization, but also a computational tool for developing and testing new hypotheses about brain function.

Keywords: Mesoscopic neurodynamics, Dissipative neural fields, Spontaneous symmetry breaking, Long-range correlations, Collective modes

1 Introduction

A century after Walter Freeman's birth, one of the questions that guided much of his scientific work remains remarkably open: how does the physical activity of the brain self-organize into coherent, spatially extended population dynamics capable of supporting perception, meaning and adaptive behavior? In *Mass Action in the Nervous System* [1], Freeman framed the brain as a physicochemical system whose local components had to be understood together with the principles governing their collective organization; we would say their architecture. His subsequent work pursued this question across neurophysiology, nonlinear dynamics and theoretical neuroscience, with particular attention to the emergence of meaning and intentional behavior from the coordinated activity of neuronal populations [2–5]. The breadth of this program is especially relevant here because it placed the relation between local neural processes and global organization, rather than each level in isolation, at the center of the problem.

Freeman's experimental approach to the study of brain provided a concrete expression of this view. Cortical activity was found to organize rapidly into spatially extended amplitude-modulated patterns, coordinated oscillatory domains and transient wave packets, separated by abrupt dynamical transitions [6]. Such phenomena motivated his concept of *mesoscopic neurodynamics* [2]: a level of description intermediate between individual neurons and the brain as a whole, at which population activity acquires spatial and temporal organization not attributable to any isolated cell [7–9]. The resulting problem is therefore not simply how individual neurons respond, but how many interacting neural degrees of freedom can generate coherent states and transitions belonging to the neural population as a whole.

This question has a natural counterpart in many-body physics. There, macroscopic organization is described through collective variables, order parameters and collective modes: dynamical properties that characterize an interacting system without being reducible to the state of any individual constituent. The quantum-field-theoretic brain model introduced in 1967 by Ricciardi and Umezawa [10–12] applied this perspective to neural dynamics by proposing that functional brain states could be represented as macroscopically ordered states of many interacting degrees of freedom (see also [13–15]). Different microscopic configurations may then correspond to the same macroscopic organization, shifting the relevant description from individual components to collective variables.

Within quantum field theory, this transition is associated with spontaneous symmetry breaking and the emergence of long-range correlations and Nambu–Goldstone modes [16–20]. The order parameter identifies the macroscopically selected state, while collective excitations describe coordinated degrees of freedom that remain dynamically active around that ordered configuration. The dissipative extension developed by Vitiello (1995) [21–23] introduced the openness of the brain to its environment, and Freeman and Vitiello later related this many-body framework to the observed formation and reorganization of mesoscopic cortical patterns [8, 9, 24, 25]. Pessa and Vitiello (1999) [26–28] (see also [29]) further showed that related structural principles could be formulated explicitly in a neural-network setting using complex doublet variables and

collective order parameters. These developments provide the theoretical background for the present work.

A substantial gap nevertheless remains between the infinite-system framework of quantum field theory and an explicitly finite computational model. Such a model would be of paramount importance to understand neural activity by simulation and experiment. Spontaneous symmetry breaking, unitarily inequivalent representations and Nambu–Goldstone modes have precise meanings in the thermodynamic or infinite-volume limit. A finite lattice cannot simply be assumed to instantiate these properties. This does not mean, however, that *signatures of collective organization cannot be identified in a finite dissipative system.*

In this paper, we address this question using a *dissipative neural field* realized through a finite two-dimensional lattice of normalized complex doublets. Each site defines three local $SU(2)$ observables, whose sums provide global collective variables. Specifically, we study the properties of collective organization of this model, including the input-induced selection of a macroscopic ordered state, the growth of the order parameter with system size together with decreasing relative fluctuations, the persistence of active degrees of freedom around the established order, and the emergence of long-range correlations extending beyond the range of direct local interaction. The central question of the paper is therefore whether a finite dissipative neural field can exhibit a transition from local dynamics to macroscopic order, and from macroscopic order to extended collective organization, like the one observed in the brain.

Our model abstracts a few but relevant computational principles from Quantum Field Theory. Long-range structures observed in the finite model are investigated as *finite-system candidate signatures of collective-mode organization.* In this sense, the model provides an operational bridge between the many-body framework of Quantum Field Theory and Freeman's view of brain function as emerging from the organized dynamics of neural populations [8, 9].

The presentation plan is as follows. In Section 2, structural algebraic aspects of spontaneous breakdown of symmetry, the Goldstone theorem, and the dynamical generation of long-range correlations in QFT are briefly presented. The finite-lattice realization of our dissipative neural field model is discussed in Section 3, where some mathematical features of the model are also discussed, in view of the numerical analyses and methods to which Section 4 is devoted. In Section 5, the results of our analysis are presented. There we show the emergence of macroscopic order (in the longitudinal direction), the persistence of collective modes in the transverse sector with consequent long-range transverse organization in the net activity. The dissipative character of the model dynamics is crucial in the derivation of our results. The stress is on the appearance of collective modes, thus showing the net not simply as a collection of field activities at the net distinct sites, but rather as long-range correlated site domains characterizing global net properties, thus differing from conventional studies of finite lattice nets. Sections 6 and 7 are for final discussion and conclusions. Mathematical formalism and technical issues entering our analyses can be found in the Appendices A-D.

2 Spontaneous Breakdown of Symmetry and Collective Modes

This section aims to introduce the main concepts of quantum field theory (QFT) needed for the subsequent analysis of collective organization in classical finite-lattice neural nets.

The spontaneous breakdown of symmetry (SBS), together with the Goldstone theorem and the related phenomenology, has played a central role in the development of many-body and elementary-particle physics, with extensions to condensed matter, biological systems and neuroscience. Its relevance here lies primarily in the possibility of describing how the dynamics of many interacting microscopic components can give rise to ordered macroscopic states and collective modes [16–20].

One of the most important consequences of SBS is indeed the dynamical emergence of collective modes associated with long-range correlations among the elementary components of a system. In the field-theoretic description, the quanta of these correlations are the Nambu–Goldstone (NG) modes. Their coherent condensation provides the ordered background through which microscopic dynamics can manifest itself as macroscopic, effectively classical behavior. Familiar examples of collective excitations include magnons in magnetic systems and phonons in crystals.

The degree of macroscopic ordering is characterized by an *order parameter*, defined as the expectation value of a suitable field or collective observable. Although rooted in the microscopic dynamics, the order parameter behaves macroscopically as an effectively classical quantity controlling the ordered state of the system. Magnetization in a ferromagnet provides the paradigmatic example: the microscopic interactions remain rotationally symmetric, whereas the ordered state selects a definite macroscopic direction.

More generally, SBS occurs when the dynamical laws remain invariant under the transformations of a symmetry group G, while the vacuum state is invariant only under a subgroup $G^{'} \subset G$. The symmetry is said to be spontaneously broken because the ordered state is selected dynamically rather than by an explicit asymmetry in the underlying laws. An external source may nevertheless act as a symmetry-breaking perturbation, allowing the system to access one among the available ordered sectors.

In QFT, distinct ordered phases may correspond, in the infinite-volume limit, to unitarily inequivalent representations of the canonical commutation or anticommutation relations, each characterized by its own vacuum state. This distinguishes the field-theoretic many-body setting from ordinary quantum mechanics with a finite number of degrees of freedom, where, under the assumptions of the Stone–von Neumann theorem [30], the irreducible representations of the canonical commutation relations are unitarily equivalent.

Ricciardi and Umezawa[10–12] recognized that this formal structure could provide a model of collective neural organization. In their 1967 proposal, information recording was associated with the formation of an ordered state through SBS and the corresponding condensation of NG collective modes. The functional state of the system was therefore represented not by the configuration of individual neural elements, but by a macroscopic order parameter characterizing the system as a whole.

The original Ricciardi–Umezawa model did not, however, explicitly incorporate the openness of the brain, which continuously exchanges energy, matter and information with its environment. The dissipative extension introduced by Vitiello addressed this point by embedding the neural system within a larger dynamical description that includes its environment [21, 22]. In the canonical treatment, this is achieved by doubling the system degrees of freedom: to each physical degree of freedom A one associates a corresponding tilde degree of freedom $\widetilde{A}$, so that the combined system $\{A, \widetilde{A}\}$ can be treated as closed while allowing energy and information exchange between its two sectors. A closely related doubling construction is used in finite-temperature QFT. The formal dissipative structure relevant to the present model is discussed in Appendix C.

An important consequence of the dissipative extension was the enlargement of memory capacity. In the original Ricciardi–Umezawa model, successive information inputs act within the same representation and may therefore interfere with previously established condensates. In the dissipative formulation, different information codes can instead label different ordered vacua belonging, in the infinite-volume limit, to unitarily inequivalent representations. This historical development is important for the origin of the model considered here, although the present work focuses not on memory capacity itself but on the emergence and organization of collective modes.

A further feature of the symmetry-breaking construction is particularly relevant to the analyses developed below. Once an ordered direction has been selected, the order parameter defines a *longitudinal sector*, whereas the broken directions identify a *transverse sector* (cf. Appendix B). In the QFT formulation, the NG modes and the associated long-range correlations reside in these transverse degrees of freedom. Our finite model therefore examines not only whether a macroscopic ordered component develops, but also whether transverse degrees of freedom remain dynamically active and acquire collective and spatially extended organization.

In the following sections, inspired by the dissipative model of the brain, we study a neural net as a system open to its environment, from which it receives inputs. These break the symmetry, with consequent formation of long-range correlations and collective modes.

Table 1 summarizes the correspondence between the main theoretical objects introduced above and their finite-lattice realizations, which are defined explicitly in Section 3. The source perturbation tests whether the implemented field can enter an ordered sector, while the subsequent analyses examine the collective properties supported by that ordered medium.

Throughout the paper we therefore distinguish two levels of description: the local degrees of freedom associated with the individual lattice sites, and the collective variables characterizing the neural field as a whole. Collective modes belong to the latter level: they are properties of the organized system and cannot, by definition, be assigned to any single constituent. The algebraic structures underlying this correspondence, including the large-N $SU(2)$ construction and its group contractions [31, 32], are discussed in Appendix A.

Table 1 Correspondence between theoretical objects in the many-body framework and their finite-lattice realization

Theoretical object	**Finite-lattice realization**	**Role**
Local doublet field $\psi(\mathbf{x})$	$\psi_r(t) \in \mathbb{C}^2$	Local field variable
Local generators	$s_i(r,t)$	Local observable
Global generators	$S_i(t) = \sum_r s_i(r,t)$	Collective observable
Order parameter	$S_3,\ m_3 = S_3/N$	Longitudinal macroscopic order
Broken/transverse sector	$\mathbf{s}_\perp = (s_1, s_2)$	Candidate collective-mode channel
External perturbation	$P_r(t)$	Order selection and controlled field reorganization

3 A Finite-Lattice Realization of a Dissipative Neural Field Model

The theoretical framework outlined above describes neural organization in terms of local $SU(2)$ degrees of freedom, macroscopic order and collective correlations. To examine which aspects of this structure can be made operational in a finite system, we use a dissipative neural field defined on a two-dimensional lattice. The model is not intended as a finite simulation of quantum field theory of the brain in the strict sense. Rather, it preserves selected structural elements of the many-body framework - including local complex doublets, $SU(2)$ observables, global order variables, spatial coupling, dissipation and externally driven reorganization - and expresses them through finite quantities that can be directly measured. It is important to note that the lattice itself should not be interpreted as a microscopic reconstruction of cortical tissue. A site represents a local neural degree of freedom at the level of the model and may be viewed as a coarse-grained state associated with a local population or neural region rather than with a single biological neuron.

The purpose of this section is therefore to establish the correspondence between the theoretical description and the finite dynamical system analyzed below. In particular, the model allows us to ask whether an initially unbiased field can develop macroscopic order under an external symmetry-breaking perturbation, how that order scales with system size and whether the resulting ordered state supports extended organization in the transverse sector. These questions define the link between the many-body framework and the numerical analyses presented in Section 4.

3.1 The FIELD model

The model, implemented and discussed by Terenzi [33], is defined on a two-dimensional periodic lattice

$$\Lambda_L = \mathbb{Z}_L \times \mathbb{Z}_L, \qquad N = \mid \Lambda_L \mid = L^2, \tag{1}$$

where L is the linear lattice size and N the total number of sites. Periodic boundary conditions make the lattice topologically equivalent to a discrete torus, avoiding

boundary-specific effects and allowing spatial relations to be treated uniformly across the field.

Each lattice site $r \in \Lambda_L$ carries a complex two-component vector

$$\psi_r(t) = \begin{pmatrix} \psi_{r,+}(t) \\ \psi_{r,-}(t) \end{pmatrix} \in \mathbb{C}^2. \tag{2}$$

The $\pm$ components define the two internal degrees of freedom of the local doublet. Their amplitudes are continuous and satisfy the normalization condition

$$\| \psi_r(t) \|^2 = | \psi_{r,+}(t) |^2 + | \psi_{r,-}(t) |^2 = 1. \tag{3}$$

Thus, at each site, the doublet field may be in its $+$ or $-$ component. After removal of an irrelevant overall phase, the local doublet can equivalently be represented as a point on the Bloch sphere,

$$\psi_r(t) \in \mathbb{C}^2/U(1) \simeq S^2. \tag{4}$$

The complete configuration of the system at time t is the lattice field

$$\psi(t) = \{\psi_r(t)\}_{r \in \Lambda_L}. \tag{5}$$

The doublet is used here as a finite field variable carrying the $SU(2)$ structure introduced in Section 2. Its use does not require the individual lattice sites to be interpreted as microscopic quantum neurons.

Through the Pauli matrices σ_i, $i = 1, 2, 3$, the complex doublet at each site and time t can be mapped onto the real local $SU(2)$ generators

$$\mathbf{s}(r,t) = (s_1, (r,t), s_2(r,t), s_3(r,t)) \tag{6}$$

where

$$s_i(r,t) = \psi_r^\dagger(t) \frac{\sigma_i}{2} \psi_r(t), \qquad i = 1, 2, 3, \tag{7}$$

i.e., explicitly,

$$s_1(r,t) = Re\left[\psi_{r,+}^*(t)\psi_{r,-}(t)\right], \qquad s_2(r,t) = Im\left[\psi_{r,+}^*(t)\psi_{r,-}(t)\right], \tag{8}$$

and

$$s_3(r,t) = \frac{1}{2}(| \psi_{r,+}(t) |^2 - | \psi_{r,-}(t) |^2). \tag{9}$$

The third component s_3 measures the local polarization along the internal $+/-$ axis which is denoted as the *longitudinal* sector. The first two components describe the orthogonal, or *transverse*, sector,

$$\mathbf{s}_\perp(r,t) = (s_1, (r,t) s_2(r,t)). \tag{10}$$

This distinction will be central below. Once macroscopic order develops predominantly along the third direction, s_3 provides the local contribution to the ordered sector, whereas s_1 and s_2 describe the transverse degrees of freedom in which collective

reorganization can be examined. The reason for focusing on the transverse sector is that changes along that direction primarily modify the magnitude of the order parameter itself, whereas transverse variations can reorganize the local configuration while largely preserving the established order. In many-body systems with a broken symmetry, such transverse degrees of freedom are therefore the natural channel in which collective fluctuations and extended correlations are expected to appear.

Global generators are obtained by summing the local components over the lattice,

$$S_i(t) = \sum_{r \in \Lambda_L} s_i(r,t), \qquad i = 1,2,3, \tag{11}$$

with corresponding quantities

$$m_i(t) = \frac{S_i(t)}{N}. \tag{12}$$

The relation between the local doublets and the longitudinal global variable can also be written by defining the populations

$$N_+(t) = \sum_{r \in \Lambda_L} \mid \psi_{r,+}(t) \mid^2, \qquad N_-(t) = \sum_{r \in \Lambda_L} \mid \psi_{r,-}(t) \mid^2, \tag{13}$$

with

$$N_+(t) + N_-(t) = N, \tag{14}$$

and therefore

$$S_3(t) = \frac{1}{2}\left[N_+(t) - N_-(t)\right], \tag{15}$$

which provides the finite-lattice counterpart of the polarization variable introduced in the theoretical framework. We therefore use

$$M(t) \equiv S_3(t) \tag{16}$$

as the extensive order variable and its density

$$m_3(t) = \frac{S_3(t)}{N}. \tag{17}$$

This formulation is useful because a given value of S_3 does not specify a unique microscopic lattice configuration. Many different distributions of local doublets may yield the same global order. The finite model therefore preserves the distinction, central to the many-body description, between microscopic configuration and macroscopic state.

The three global components also distinguish an ordered longitudinal direction from a transverse sector with S_3 as the longitudinal order and (S_1, S_2) as the transverse sector. The purpose of the numerical analysis is not merely to determine whether S_3 becomes non-zero, but to test whether it behaves increasingly as a macroscopic

variable as N grows and whether extended organization develops in the transverse field around the selected ordered direction.

We remind that the correspondence between the main theoretical quantities introduced in Section 2 and their finite-lattice realization is summarized in Table 1. The mapping is not intended as an identification between the model and the full quantum-field-theoretic construction. Rather, it specifies which structural elements of the many-body framework are retained as explicit, measurable quantities in the lattice model.

The lattice evolves through a driven and spatially coupled non-unitary update. In schematic continuous-time form,

$$\dot{\psi}_r = c(\Delta\psi)_r - \gamma_r\psi_r + i\omega_r\psi_r + P_r(t) + R_r(t), \tag{18}$$

where Δ is the discrete toroidal Laplacian that couples nearest-neighbour sites, $\gamma_r\psi_r$ is the dissipative relaxation, $i\omega_r\psi_r$ is the local phase rotation, $P_r(t)$ represents the externally applied perturbation, and $R_r(t)$ collects protocol-dependent terms used in specific simulations.

Numerical integration is followed by local normalization of the complex doublet. Consequently, the term $-\gamma_r\psi_r$ should not be interpreted as a directly observable decay of the local norm: normalization constrains that norm by construction. It acts within the pre-normalized update and in competition with the other dynamical contributions. The present implementation should therefore be regarded as an effective dissipative neural-field dynamics.

A source perturbation along the third internal direction is used to select an S_3 -ordered state. Specifically, external inputs enter through the drive $P_r(t)$. A symmetry-selecting *source pulse* applied along the third internal direction can be written schematically as

$$P_{src}(r,t) \propto \varepsilon_3(r,t)\ \sigma_3\psi_r(t), \tag{19}$$

where $\varepsilon_3(r,t)$ specifies its spatial and temporal profile, which might also be independent of space and time. Essential requirement is that it acts as a trigger and it goes to zero after its action. Its role in the present work is to test whether an initially unbiased finite field can be driven into a macroscopically S_3 -ordered sector and whether that order persists after the transient perturbation.

Subsequent structured perturbations act on the already ordered field and are used here as controlled probes of its reconfiguration. Their role in the present paper is not to implement symbolic computation, but to generate reproducible field trajectories through which longitudinal, transverse and spatially extended dynamics can be examined

4 Numerical Methods

4.1 Experimental logic

The numerical analysis was organized as a progression from local field dynamics to macroscopic and spatially extended organization. The first question was whether a transient symmetry-selecting input could drive an initially unbiased finite lattice into

a state with a preferred macroscopic order direction. We then asked whether the resulting order acquires collective scaling properties as system size increases, rather than remaining a finite-size fluctuation. Finally, we examined whether the order along the longitudinal S_3 direction leaves a non-trivial transverse sector and whether the dynamics of this sector develops correlations extending beyond the scale of direct local interaction.

These tests address two distinct but connected requirements. A non-zero value of S_3 alone is not sufficient to identify macroscopic collective organization, since any finite system may exhibit fluctuations away from zero. The relevant question is whether the selected order becomes increasingly extensive and stable relative to its fluctuations as N grows. Likewise, longitudinal order alone does not imply the presence of collective-mode dynamics. The ordered system must retain degrees of freedom transverse to the selected direction, and their organization must extend beyond purely local interactions, where, according to the Goldstone Theorem, the collective modes are expected to be found. For this reason, the analyses below distinguish the longitudinal component S_3, which provides the finite-lattice order variable, from the transverse sector represented by S_1 and S_2.

All numerical experiments were performed using the finite dissipative neural field previously defined. The same local field variables, global $SU(2)$ observables and normalization conventions were used throughout. Simulations started from approximately unbiased field configurations, with no preferred macroscopic direction, and a transient source perturbation along the third internal axis was used when an S_3-ordered state was required. After each numerical update, the local complex doublets were normalized as described in Section 3. A *frame* denotes the complete state of the lattice recorded at one discrete simulation step, including the local field variables at all sites; frame-to-frame changes therefore describe the evolution of the full spatial field between successive numerical updates.

4.2 Experimental Protocols

Several complementary protocols were used to probe different properties of the resulting ordered state. Initial order selection was examined for L=8,10,12, with eight independent realizations at each lattice size, by comparing the global order variables before and after the symmetry-selecting source. Finite-size behavior was then evaluated over the extended range

$$L = 8,\ 10,\ 12,\ 16,\ 20,\ 24,\ 28,\ 32, \qquad N = 64\text{–}1024, \tag{20}$$

using 128 independent realizations for each size and a common parameter set across the entire series. No size-dependent calibration was introduced. The principal longitudinal measures were the order density $\langle S_3\rangle/N$ and the relative fluctuation amplitude $SD(S_3)/|\langle S_3\rangle|$. Transverse collective activity was quantified through

$$Var_{\perp} = Var(S_1) + Var(S_2), \tag{21}$$

and

$$S_{\perp,rms} = \sqrt{\langle S_1^2 + S_2^2 \rangle}, \tag{22}$$

Their dependence on N was evaluated by power-law fits in order to distinguish extensive longitudinal order from the scaling of transverse fluctuations. The corresponding large-N algebraic interpretation is given in Appendix A.

The dynamical distinction between longitudinal and transverse perturbations was examined with the *Shift Test*. Once an S_3-ordered state had been established, controlled perturbations were applied either along the two transverse directions or directly along the order-defining longitudinal direction. A random perturbation provided a nonspecific control. The primary response variables were the post-relaxation changes ΔS_3 and $\Delta|S|$. In addition, we used the finite physical/tilde construction also described in Appendix C to compute the scalar response functional F^p, and its post-relaxation difference ΔF^p relative to the corresponding unperturbed ordered state. constructed from the physical/tilde doubled representation through the transport mapping described in Appendix C. In the present analysis, F^p is used only comparatively: ΔF^p measures the residual difference between a relaxed perturbed state and its unperturbed reference. F^p is a homologue of the thermodynamic free energy but should not be interpreted as a physical quantity of the underlying quantum field theory. Rather, it is used as an *effective measure of how strongly a perturbation displaces the finite ordered system.* Of particular interest is the change in F^p that remains after the external perturbation has ceased and the field has been allowed to relax. A small residual change indicates that the field has accommodated the perturbation with little alteration of the ordered state; a larger residual change indicates that the field has been driven farther away from that state.

Spatial organization of the transverse sector was analyzed relative to the *instantaneous macroscopic order direction.* At each frame, the normalized global order vector defined a longitudinal axis, and two orthogonal directions perpendicular to it defined the local transverse plane. The corresponding complex transverse field $s_\perp(r,t)$ was then used for both descriptive and spectral analyses. Long-range functional graphs were constructed only as spatial visualizations of increasing transverse similarity between distant sites; because the number of possible pairs grows strongly with lattice size, graph counts were not used as the principal quantitative evidence. The main measure was instead the transverse structure factor

$$S_\perp(\mathbf{k}) = \frac{1}{N} \mid \sum_r s_\perp(r) e^{-i\mathbf{k}\cdot r} \mid^2 \tag{23}$$

from which the fraction of non-zero-wavevector power contained in the lowest spatial modes was calculated. Small non-zero $|\mathbf{k}|$ correspond to patterns varying over the largest spatial scales available on the finite lattice.

The long-wavelength analysis used L=8,12,16,20, 32 paired random seeds (42–73), and both prescribed and permuted perturbation sequences. Spatial organization was evaluated against two matched null models. In the *spatial-shuffle null*, the complex transverse values were randomly permuted among lattice sites, preserving their distribution while destroying their spatial arrangement. In the *phase-randomized null*, the

local transverse amplitudes were retained while their phases were randomized. Three independent realizations of each null configuration were generated for every empirical frame. A further transport control set the inter-site transport coefficient to zero while adjusting the source drive so that strong longitudinal order was preserved, thereby testing whether large-scale transverse organization depended specifically on spatial coupling rather than on polarization alone.

Throughout the numerical analyses, a *seed* denotes the initial state of the random-number generator and therefore identifies one independent and reproducible simulation realization. Where confidence intervals are reported, the seed - not the individual temporal frame - was treated as the independent replication unit. For paired empirical/null comparisons, null realizations were first averaged within each lattice size, seed and branch before computing seed-level differences; 95% confidence intervals were then calculated from these independent paired differences. Further implementation and analysis details are provided in Appendices A, C and D

5 Results

5.1 Emergence of Macroscopic Order

The first result concerns the emergence of a macroscopic ordered state from an initially unbiased field. Before application of the transient symmetry-selecting source, the three global components were numerically close to zero,

$$S_1(0) \simeq S_2(0) \simeq S_3(0) \simeq 0. \tag{24}$$

After stimulation along the third internal direction, S_3 acquired a macroscopically non-zero value. In the initial L = 8,10,12 series, both S_3 and the magnitude of the global order vector increased with lattice size (Table 2; Fig. 1), showing that the external input consistently selected an S_3-ordered sector.

Table 2 Initial finite-size series showing input-induced selection of S_3 order

L	$N = L^2$	**Cases**	$S3$ **pre**	$S3$ **post**	$\lvert S\rvert$ **post**
8	64	8	-2.78E-17	14.08	15.313
10	100	8	-6.00E-16	22.198	24.406
12	144	8	-9.99E-16	33.011	35.422

This series of experiments establishes order selection; scaling exponents are estimated from the protocol reported in Section 4

The extended finite-size analysis showed that this ordered component behaves increasingly as a macroscopic collective variable as system size grows. The longitudinal order density remained approximately size-independent,

$$\frac{\langle S_3 \rangle}{N} \simeq 0.179, \tag{25}$$

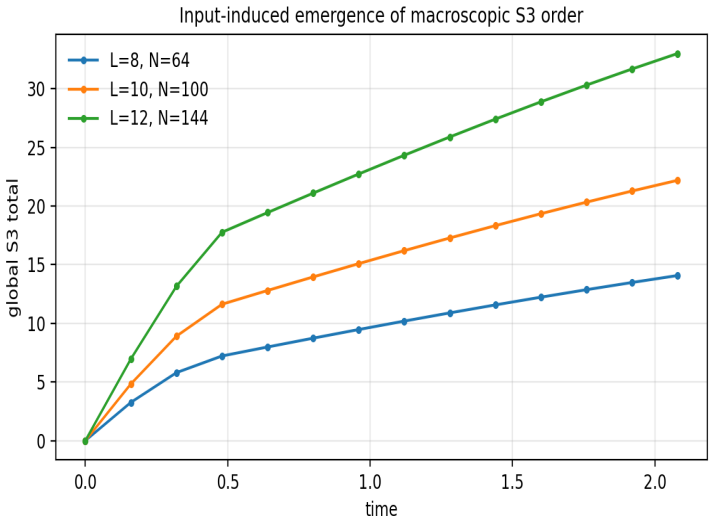


Fig. 1 Input-induced selection of macroscopic S_3 order. Evolution of the global longitudinal component in the initial $L = 8,\ 10,\ 12$ series. The source perturbation selects the third internal direction from an initially unbiased state. Quantitative finite-size scaling of the ordered state is examined separately in Section 4

whereas the relative fluctuations of S_3 decreased according to

$$\frac{SD(S_3)}{\mid \langle S_3 \rangle \mid} \propto N^{-0.504}, \qquad (R^2 = 0.983), \tag{26}$$

where R^2 denotes the coefficient of determination. Thus, the ordered component grows extensively, $S_3 = O(N)$, while its fluctuations become progressively smaller relative to the mean order (Fig. 2). The observed exponent is close to the $N^{-1/2}$ scaling expected when an extensive collective quantity is accompanied by fluctuations of order $\sqrt{N}$.

5.2 Persistence and Collective Scaling of the Transverse Sector

Macroscopic longitudinal ordering did not suppress the remaining transverse degrees of freedom. In the extended finite-size series,

$$Var_{\perp} = Var(S_1) + Var(S_2) \propto N^{1.022}, \qquad R^2 = 0.992, \tag{27}$$

while

$$S_{\perp,rms} = \sqrt{\langle S_1^2 + S_2^2 \rangle} \propto N^{0.515}, \qquad R^2 = 0.993. \tag{28}$$

The characteristic transverse amplitude therefore grows approximately as $\sqrt{N}$, whereas the longitudinal ordered component grows as N. The normalized quantities reported in Table 3 remain correspondingly stable over L=8–32. The ordered lattice

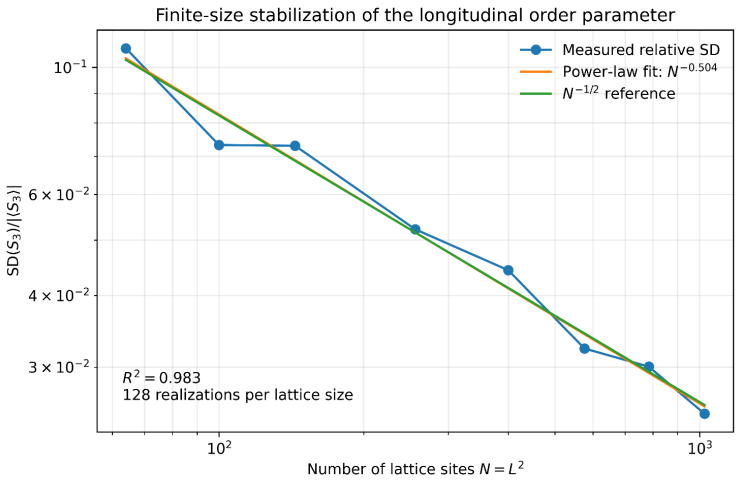


Fig. 2 The empirical and $N^{-1/2}$ reference trends are superimposed. Relative standard deviation of the global longitudinal component S_3 across 128 independent realizations for lattice sizes $L = 8$ –32 ($N = 64$ –1024). The measured relative fluctuations decrease as $N^{-0.504}$ ($R^2 = 0.983$), closely following the $N^{-1/2}$ reference scaling expected for an extensive order parameter with $\sqrt{N}$ -scale fluctuations.

therefore does not collapse into a single scalar degree of freedom: an $O(N)$ longitudinal background coexists with an $O(\sqrt{N})$ collective transverse fluctuation sector (Figs. 2–3; Table 3).

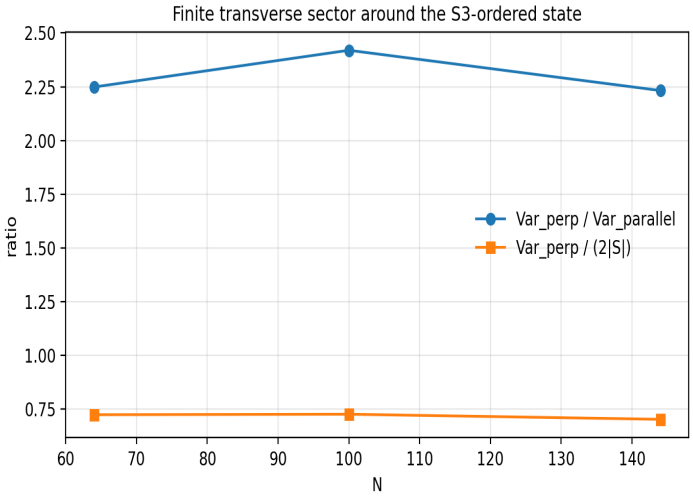


Fig. 3 Persistence of the transverse sector after macroscopic ordering. The transverse sector remains finite after reordering: it does not collapse with the emergence of S_3 order, indicating that the emergence of longitudinal order does not eliminate transverse field structure.

Table 3 Finite-size scaling of longitudinal order and transverse collective fluctuations

L	N	$\langle S_3 \rangle / N$	$\mathrm{Var}_\perp / N$	$S_{\perp,\mathrm{rms}}/\sqrt{N}$	$\sqrt{N} \times SD(S_3$
8	64	0.1773	0.0322	0.1789	0.8637
10	100	0.1806	0.0366	0.1915	0.7322
12	144	0.1793	0.0352	0.1872	0.8759
16	256	0.1799	0.0291	0.1699	0.8349
20	400	0.1793	0.0370	0.1919	0.8853
24	576	0.1793	0.0370	0.1926	0.7757
28	784	0.1794	0.0321	0.1818	0.8414
32	1024	0.1792	0.0377	0.1955	0.7958

The normalized quantities show that the longitudinal order density remains approximately constant with system size, while relative fluctuations decrease with the expected collective scaling and transverse fluctuations remain finite on the $\sqrt{N}$ scale. Here $\mathrm{Var}_\perp = \mathrm{Var}(S_1) + \mathrm{Var}(S_2)$.

The above-mentioned Shift Test showed that this geometrical distinction is accompanied by a clear dynamical asymmetry. Transverse perturbations along σ_1 and σ_2 produced almost no persistent change in either S_3 or $|S|$, with ΔS_3 = -0.011 and -0.032, respectively, and $\Delta|S| = 0$ in both cases. Their residual response in the doubled-field functional was likewise small, ΔF^p =-0.014 and -0.010.

Longitudinal perturbations produced a qualitatively different response. The z^+ perturbation yielded $\Delta S_3 = 0.875$, $\Delta|S| = 0.871$, and $\Delta F^p = 2.308$, whereas the z^- perturbation produced ΔS_3 = -1.173, $\Delta|S|$ =-1.166, and $\Delta F^p = 3.339$. The random perturbation remained close to the transverse responses, with ΔF^p = -0.029, ΔS_3 = 0.012, and $\Delta|S| = 0.018$ (Table 4; Fig. 4).

Table 4 Shift test separating transverse and longitudinal perturbations

Shift	ΔF^p	ΔS_3	$\Delta\lvert S\rvert$
$\boldsymbol{\sigma_1}$	-0.014	-0.011	0.000
$\boldsymbol{\sigma_2}$	-0.010	-0.032	0.000
random	-0.029	0.012	0.018
long-$\mathbf{z}+$	2.308	0.875	0.871
long-$\mathbf{z}-$	3.339	-1.173	-1.166

Comparison of the post-relaxation change in F^p, S_3, and $|\,\mathbf{S}\,|$ across perturbation directions.

These results show that the ordered field is dynamically anisotropic. Transverse perturbations can be accommodated mainly through internal reorganization around the established macroscopic state, whereas perturbations directed along the order-defining axis displace the order parameter itself and leave a substantially larger post-relaxation response.

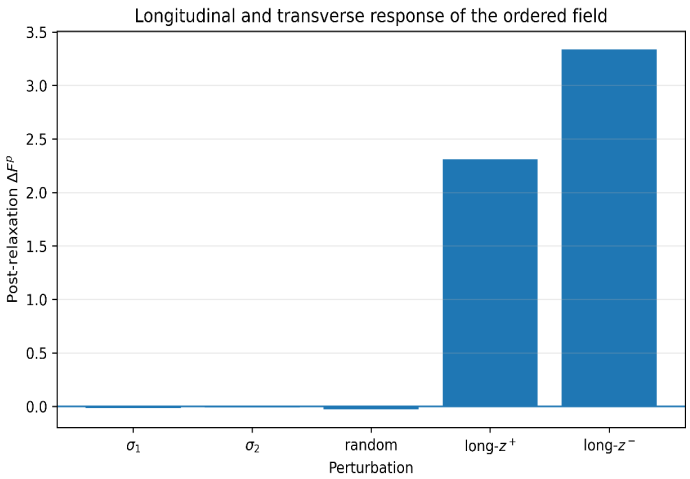


Fig. 4 Dynamical response of the ordered field to transverse and longitudinal perturbations. Post-relaxation change in the effective free-energy-like quantity F^p following controlled perturbations of the S_3 -ordered field. Transverse σ_1 and σ_2 perturbations produce only small residual changes in F^p , whereas longitudinal z^+ and z^- perturbations produce substantially larger changes. The random perturbation provides a nonspecific control. The quantity ΔF^p is used here as a comparative response measure and is not interpreted as a thermodynamic free-energy difference.

5.3 Long-Range Transverse Organization

The persistence and dynamical flexibility of the transverse sector raised the further question of whether its organization remains local or extends across substantial portions of the lattice. Functional-graph representations provided a first visualization of dynamically increasing transverse similarity between spatially distant sites (Fig. 5). They were obtained after macroscopic order has been established. Edges connect spatially distant sites whose normalized transverse similarity increases relative to the preceding frame; each edge is weighted by the magnitude of this positive increase. The lattice projection shows the weighted degree of each site, obtained by summing the weights of all incident long-range edges, and therefore its participation in the newly emerging long-range transverse organization. These graphs were used just descriptively and do not constitute the principal finite-size measure, as the number of possible long-range pairs increases with lattice size.

Instead, the quantitative test is provided by the spectral analysis. Across L=8,12,16,20, the empirical transverse field contained more power in the lowest nonzero spatial modes than the matched spatial-shuffle null models. After averaging lattice sizes within each seed, the empirical excess was

$$\Delta f_{(low-k)} = 0.0139, \qquad 95\%CI = [0.0084, 0.0193]. \tag{29}$$

The phase-randomized null model produced the same qualitative result. Thus, the observed low-k organization cannot be explained simply by the distribution of local

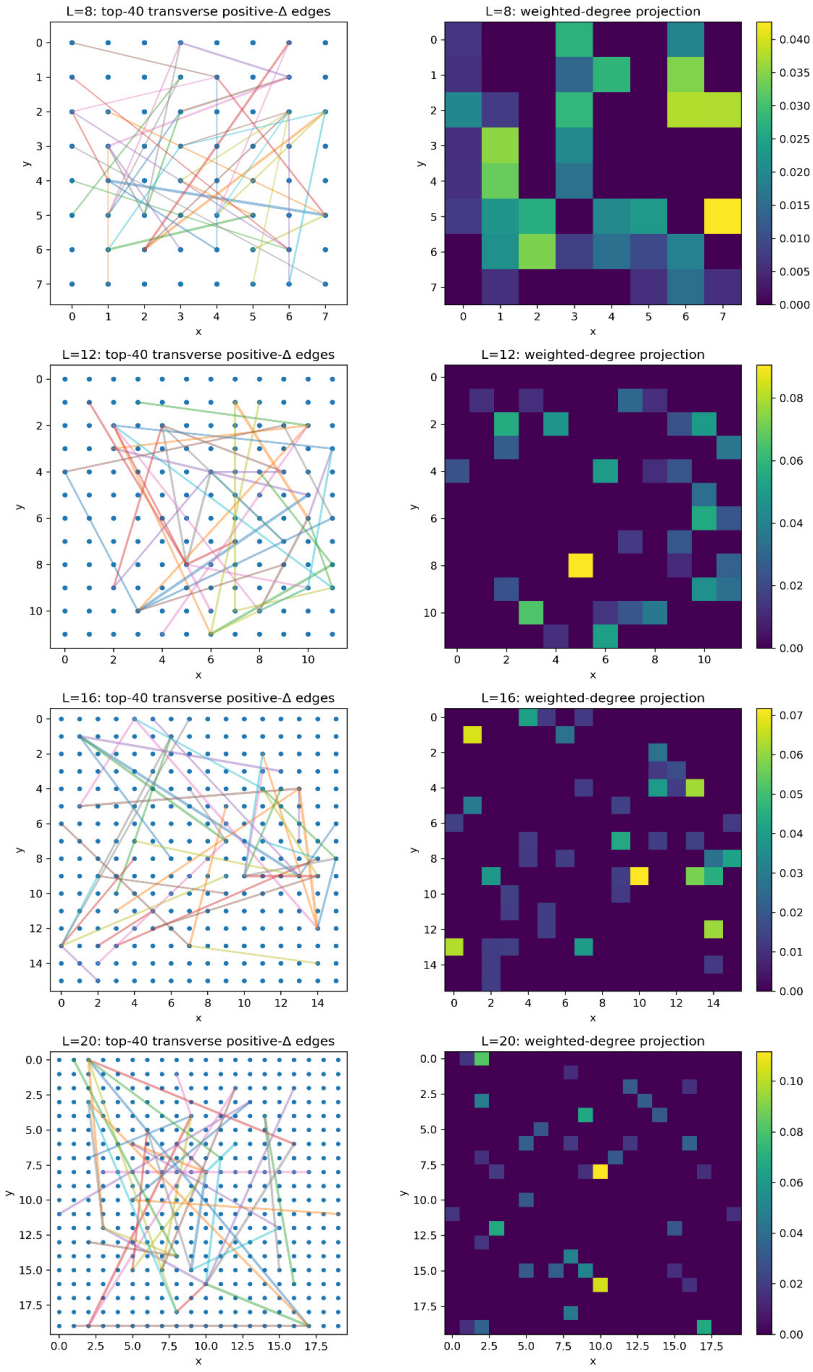


Fig. 5 Representative long-range functional organization of the transverse sector.

transverse amplitudes; it depends on their spatial arrangement and phase relationships (Fig. 6). A transport control further separated spatial collective organization from

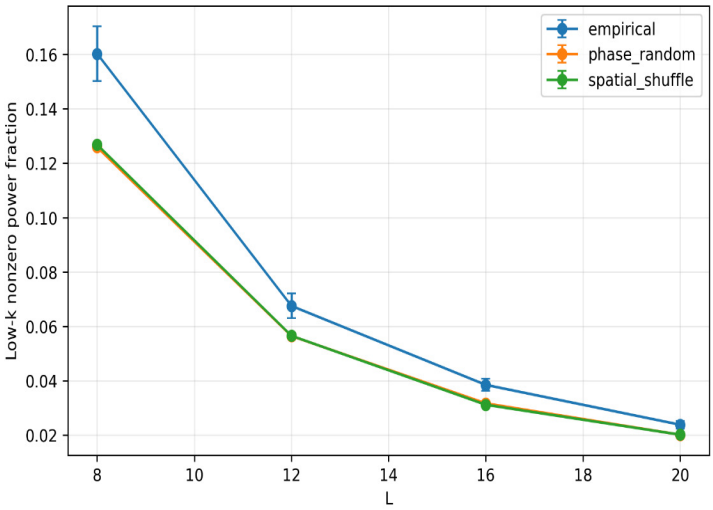


Fig. 6 Long-wavelength transverse organization relative to spatial null models. Fraction of non-zero-wavevector transverse power contained in the lowest spatial modes ($k^2 \leq 2$) for the empirical canonical-field dynamics and matched spatial-shuffle, and phase-randomized null models. Low-k modes correspond to transverse structures varying over the largest spatial scales available on the finite lattice. The empirical field shows a systematic excess of low-k power across lattice sizes, indicating spatial organization not explained by the distribution of local transverse amplitudes alone.

macroscopic polarization alone. When spatial transport was removed while the source drive was increased to preserve strong S_3 polarization, the low-k excess was strongly reduced and no longer consistently separated from the null distributions. Correct and permuted action sequences, by contrast, produced comparable total low-k organization. The phenomenon therefore appears to characterize the spatially extended substrate of the driven transverse dynamics rather than the correctness of a particular perturbation sequence. More details can be found in Appendix D.

Taken together with the collective $\sqrt{N}$ transverse scaling and the Shift Test, this transport-dependent long-wavelength organization provides the strongest finite-size evidence in the present model for candidate collective-mode behavior.

6 Discussion

The neural-network architecture studied here differs from conventional approaches in many respects, but mainly for the choice of its elementary dynamical variables. Rather than representing the system only through scalar unit activations and weighted connections, each lattice site carries a complex $SU(2)$ doublet whose evolution contributes

to a dissipative spatial field. The relevant state of the system is therefore specified not only by its local variables, but also by the collective organization that emerges from their interaction. Here, a lattice site should not be identified with a single biological neuron; on the contrary, it is better regarded as a coarse-grained local neural degree of freedom, potentially representing a small population or local region embedded in a larger neural medium. Neurons, synaptic interactions, and external contributions would constitute the underlying biological substrate, whereas order parameters, spatial modes, and field trajectories belong to a mesoscopic level of description.

This distinction closely reflects Walter Freeman's emphasis on *mass action* and mesoscopic neurodynamics. In his experimental work, cortical function was associated not simply with the activity of individual neurons, but with rapidly formed, spatially extended amplitude-modulation patterns, structured phase organization and transient wave packets involving large neuronal populations. The present model does not attempt to reproduce these electrophysiological phenomena literally. Indeed, its variables are not EEG variables, and the lattice is not a geometrical reconstruction of cortex. The correspondence is, instead, dynamical and organizational. Local degrees of freedom give rise to an ordered population-level state that remains internally structured and capable of rapid collective reconfiguration.

Also, our perturbation protocol can be interpreted within this framework. The initial source acts as a controlled input that drives an initially unbiased neural medium toward a macroscopically ordered state, while subsequent structured perturbations probe how that already organized field can be reconfigured. The ordered sequences used in the simulations should therefore not be interpreted as symbolic operations literally performed by cortical neurons. They provide reproducible external or internal drives through which different trajectories of the same organized field can be examined. What matters is not simply which local units are activated, but how their states become incorporated into population-level organization and how that organization evolves in time.

The interpretation in terms of collective modes rests on the convergence of several results. The longitudinal component grows extensively with system size, while transverse fluctuations remain finite on the collective $\sqrt{N}$ scale. The Shift Test shows that these transverse degrees of freedom can reorganize substantially while producing little change in the macroscopic order parameter, whereas perturbations acting directly along the ordered direction produce much larger residual displacements. Finally, the transverse field contains more long-wavelength spatial organization than expected from matched null models, and this organization is strongly reduced when spatial transport is removed. The ordered field therefore combines stable macroscopic polarization with a dynamically active and spatially organized transverse sector. It is the conjunction of the studied properties, rather than any single measurement, that motivates their interpretation as candidate finite-size signatures of collective-mode organization. In the many-body framework, collective modes are coordinated degrees of freedom belonging to the organized system as a whole rather than to any individual constituent. Freeman's mesoscopic neurodynamics similarly emphasizes spatially extended population states rather than isolated neuronal events.

Long-range organization should also not be identified with uniform synchronization. Freeman's wave packets and phase patterns were spatially textured states, and the spectral results obtained here point in the same general direction: large-scale organization can involve structured variations of phase and sign across the field rather than homogeneous coherence. The transport control further shows that global polarization and spatial collective organization are distinct properties. A field may remain strongly ordered while losing much of the long-wavelength transverse structure generated by spatial interaction.

This perspective suggests a level of neural description intermediate between microscopic neuron-based models and purely macroscopic field variables. Interactions among local neural elements may generate mesoscopic variables - order parameters, spatial modes, transient domains and trajectories - that become relevant dynamical objects in their own right. The main challenge is therefore also experimental. Indeed, the latent variables of the model cannot be identified directly with membrane potentials, spikes or extracellular voltages. Explicit *observation operators* are required to determine how field variables and collective modes would appear in experimentally accessible population signals such as MEA, EEG or ECoG recordings.

7 Conclusions

This study examined whether a neural architecture formulated as a dissipative SU(2) doublet vector field on a finite lattice can support a transition from local degrees of freedom to mesoscopic collective organization. The results indicate that these two descriptive levels can coexist within the same dissipative dynamical system. Local doublet states give rise to a macroscopic ordered sector, while transverse degrees of freedom remain dynamically active, display collective scaling, respond differently from the longitudinal sector, and develop spatial organization extending over large fractions of the lattice. The resulting picture is therefore not one of a field collapsing into a single global variable, but of an ordered dissipative neural medium that retains structured collective freedom.

This architecture is relevant to brain dynamics because it provides a concrete computational realization of the distinction between local neuronal activity and the mesoscopic organization of neuronal populations. The lattice used here is not intended as a literal reconstruction of cortical tissue, nor should individual sites be identified with individual neurons. Rather, the model represents a dissipative coarse-grained neural medium in which local states interact and generate population-level variables. The relation to Freeman's work is therefore structural. Even though the implementation of the model discussed here does not reproduce cortical wave packets, amplitude-modulation patterns or phase cones, it captures several organizational principles that were central to his account of brain dynamics, namely the emergence of population-level order, the persistence of internal degrees of freedom within ordered states, rapid reconfiguration under perturbation, and spatially extended coordination. The observation that long-wavelength transverse organization depends on spatial transport

further suggests that global order alone is insufficient to characterize mesoscopic neural dynamics; the way activity is distributed and propagated through the medium is equally important.

These conclusions must remain limited by the nature of the model. The lattice is finite and abstract, the local variables are not biophysical constructs, and the dissipative dynamics and external pulses are phenomenological constructions rather than detailed models of membrane, synaptic or extracellular physiology. Likewise, the finite-size signatures reported here do not establish spontaneous symmetry breaking in the thermodynamic limit and do not amount to proof of a non-decaying long-range correlation function. Notwithstanding this fact, the spectral results support spatially extended, long-wavelength organization.

Future work should therefore proceed in two complementary directions. On the theoretical side, larger systems, alternative geometries and coupling regimes should be explored to determine how robust the observed collective scaling and transverse organization are, and whether additional signatures of collective modes can be identified. On the neurobiological side, the most important challenge is to relate the latent variables of the model to experimentally accessible signals. This includes testing whether quantities analogous to amplitude-modulation patterns, phase organization, spatial spectra, and transient wave-packet-like transitions can be recovered through explicit observation operators. This direction is being developed in parallel in a FIELD–MEA framework aimed at linking field trajectories and collective observables to multielectrode-array recordings [34].

The present study does not establish that cortical collective dynamics is generated by the specific mechanism implemented here. It shows instead that a dissipative neural-network architecture can be constructed in which local neural degrees of freedom naturally give rise to macroscopic order, collective transverse dynamics and spatially extended organization. In this sense, the model provides a finite and testable bridge between many-body field concepts and Freeman's mesoscopic view of brain dynamics.

Funding Declaration

The authors did not receive funding supporting the preparation and submission of the present manuscript.

Appendix A. Large-N scaling and collective SU(2) structure

We start with the derivation of the SU(2) $\rightarrow$ E(2) group contraction by using solely classical vector and matricial calculus [20, 35].

For each of the $(\pm)$-components of ψ_r (cf. Eq. (2)) it is useful to adopt the notation $|+\rangle_i$ and $|-\rangle_i$, corresponding respectively to the eigenvalues $\pm\frac{1}{2}$ of the matrix $\widehat{s}^{(r)}_{3i} \equiv \frac{1}{2}\sigma_{3,i} = \frac{1}{2}(|+\rangle_{ii}\langle +| - |-\rangle_{ii}\langle -|)$, no-summation on i, where $\sigma_{3,i}$ is the Pauli matrix. The transitions between the two levels is induced by $\widehat{s}^{(r)}_{+,i} = |+\rangle_{ii}\langle -|$, and $\widehat{s}^{(r)}_{-,i} = (\widehat{s}^{(r)}_{+,i})^\dagger$. For the whole ψ-system of N elements we have the su(2) (rotational) algebra

$$[\widehat{S}_3, \widehat{S}_\pm] = \pm\widehat{S}_\pm, \qquad [\widehat{S}_+, \widehat{S}_-] = -2\widehat{S}_3, \tag{A.1}$$

with the global generators $\widehat{S}_\pm = \sum_{i=1}^N \widehat{s}_{\pm,i}$, $\quad \widehat{S}_3 = \sum_{i=1}^N \widehat{s}_{3,i}$.

The finite-lattice simulations evaluate the corresponding c-number $S_i(t)$, rather than group generators.

The free lattice dynamics was additionally tested for covariance under global $SU(2)$ rotations. For $L = 8$–32 the relative covariance error remained of order 10^{-16}, i.e. at floating-point precision. Thus, before the externally applied symmetry-selecting input, the implemented core preserves global $SU(2)$ covariance numerically.

Suppose that the transition $|-\rangle_i \to |+\rangle_i$ is induced by the external input for a number ℓ of ψ, assumed for simplicity to be originally in the same level, say e.g., the $|-\rangle_i$ level. In a realistic distribution, not all the ψ are in their $|-\rangle_i$ level. Note, however, that our conclusions are independent of our simplified initial condition [35].

We may then represent the system state as the normalized state $|\ell\rangle$:

$$|\ell\rangle \equiv \binom{N}{\ell}^{-\frac{1}{2}} \left(|-\rangle_1 ... |-\rangle_{N-\ell} |+\rangle_{N-\ell+1} ... |+\rangle_N + ... + |+\rangle_1 ... |+\rangle_\ell |-\rangle_{\ell+2} ... |-\rangle_N\right) \tag{A.2}$$

The 'polarization' of the net is given by the difference between the number of units in the $(+)$-level and $(-)$-level, i.e.,

$$\langle\ell|\widehat{S}_3|\ell\rangle = \frac{1}{2}(N_+ - N_-) = \ell - \frac{1}{2}N \ , \tag{A.3}$$

which, in the SBS terminology, is called the *order parameter*, and it is non-zero when the $SU(2)$ rotational symmetry is broken. The matrices $\widehat{S}_\pm$ give:

$$\widehat{S}_+|\ell\rangle = \sqrt{\ell+1}\,\sqrt{N-\ell}\,|\ell+1\rangle \ , \qquad \widehat{S}_-|\ell\rangle = \sqrt{N-(\ell-1)}\,\sqrt{\ell}\,|\ell-1\rangle \ . \tag{A.4}$$

By using Eqs. (A.3) and (A.4), the representation of $\widehat{S}_3$ and $\widehat{S}_\pm$ on $|\ell\rangle$ are obtained

$$\widehat{S}_3 \ = \ S^+S^- - \tfrac{1}{2}N \ , \tag{A.5}$$

$$\frac{\widehat{S}_+}{\sqrt{N}} = S^+\sqrt{1 - \frac{S^+S^-}{N}} \ , \qquad \frac{\widehat{S}_-}{\sqrt{N}} = \sqrt{1 - \frac{S^+S^-}{N}}\,S^- \ , \tag{A.6}$$

where the the definition of $\widehat{S}_\pm$ and $\widehat{S}_3$ and their algebra Eq. (A.1) imply tha $S^- = (S^+)^\dagger$, $[S^-, S^+] = 1$, and

$$S^+|\ell\rangle = \sqrt{\ell+1}|\ell+1\rangle \ , \quad S^-|\ell\rangle = \sqrt{\ell}\ |\ell-1\rangle \ , \quad S^+S^-|\ell\rangle = \ell|\ell\rangle, \quad \forall \ell. \tag{A.7}$$

Eqs. (A.5) and (A.6) are the well known Holstein-Primakoff non-linear realization of $SU(2)$ group [36, 37].

The remarkable result is that Eqs. (A.6) give for $N \gg \ell$:

$$\frac{\widehat{S}_\pm}{\sqrt{N}}\,|\ell\rangle = S^\pm\,|\ell\rangle \ . \tag{A.8}$$

By defining $S_3 \equiv \widehat{S}_3$, the su(2) algebra (A.1) therefore contracts to the (projective) e(2) (or Weyl-Heisenberg) algebra in the large N limit [20, 31, 32, 38].

$$[S_3, S^\pm] = \pm S^\pm \,, \qquad [S^-, S^+] = 1 \,, \tag{A.9}$$

the contraction parameter being $1/\sqrt{N}$, which is thus rcognized to be the natural scaling of collective transverse fluctuations. For large N, the $S^\pm$ act as ladder operators, as shwon by Eq. (A.7). Their algebraic properties are similar to the ones of the NG wave quanta B and $B^\dagger$ in the QFT formalism (cf.Appendix B).

A.1 Ordered background and collective transverse algebra

After the source pulse (or source perturbation) selects the third $SU(2)$ (internal) direction, the finite lattice develops an ordered longitudinal component

$$\langle S_3\rangle = N m_3 + o(N), \tag{A.10}$$

where

$$m_3 = \frac{\langle S_3\rangle}{N} \tag{A.11}$$

is the intensive order parameter. Numerically,

$$m_3 \simeq 0.179, \tag{A.12}$$

approximately independent of system size, and therefore

$$\langle S_3\rangle = O(N). \tag{A.13}$$

The transverse fluctuations around this ordered background are defined by

$$\delta\widehat{S}_a = \widehat{S}_a - \langle\widehat{S}_a\rangle, \qquad a = 1, 2, \tag{A.14}$$

and rescaled as

$$P_1 = \frac{\delta \widehat{S}_1}{\sqrt{N}}, \qquad P_2 = \frac{\delta \widehat{S}_2}{\sqrt{N}}. \tag{A.15}$$

If $\delta S_\perp = O(\sqrt{N})$, P_1 and P_2 remain finite as N increases. The transverse sector therefore survives as a collective fluctuation sector while remaining subextensive relative to the $O(N)$ longitudinal order.

Since subtraction of the $\langle \widehat{S}_a \rangle$ values does not modify the commutator,

$$[P_1, P_2] = i \frac{\widehat{S}_3}{N}. \tag{A.16}$$

The remaining commutators are

$$\left[\widehat{S}_3, P_1\right] = iP_2, \qquad \left[\widehat{S}_3, P_2\right] = -iP_1. \tag{A.17}$$

In the ordered large- N limit,

$$\frac{\langle S_3 \rangle}{N} \longrightarrow m_3 \neq 0, \tag{A.18}$$

and hence

$$[P_1, P_2] \longrightarrow i m_3. \tag{A.19}$$

Thus the $1/\sqrt{N}$ rescaling does not make the transverse commutator vanish. It isolates a finite collective algebra around the macroscopically ordered background.

Defining

$$Q = \frac{P_1}{\sqrt{\mid m_3 \mid}}, \qquad P = \frac{sgn(m_3) P_2}{\sqrt{\mid m_3 \mid}}, \tag{A.20}$$

gives

$$[Q, P] \longrightarrow i. \tag{A.21}$$

The transverse sector therefore approaches the Weyl–Heisenberg algebra, which may be viewed as the centrally extended, or projective $E(2)$ [32, 37, 38] structure associated with the collective large- N limit. In the QFT construction, this collective structure provides the algebraic setting for the Nambu–Goldstone boson modes discussed in Appendix B.

The role of Eq. (A18) in the present paper is more restricted. It shows that an extensive longitudinal order can coexist with finite collective transverse degrees of freedom, precisely the regime tested numerically in Section 4.

– *Geometrical Inönü–Wigner contraction*

A related but distinct road to the large-N limit is obtained by normalizing the transverse generators with the extensive radius of the collective $SU(2)$ representation. For N double-valued $SU(2)$ vectors, the maximal collective representation has

$$j_N = \frac{N}{2}, \tag{A.22}$$

and its characteristic radius is

$$R_N = \sqrt{j_N(j_N+1)} \simeq \frac{N}{2} \quad \text{for} N \gg 1. \tag{A.23}$$

We therefore use the asymptotically equivalent reference scale

$$R_N = \frac{N}{2}. \tag{A.24}$$

This is the natural radius of the maximal collective representation and is used here only as an extensive scaling reference; it does not imply that every numerical state belongs to the maximal-j sector.

Defining

$$\Pi_1 = \frac{\widehat{S}_1}{R_N}, \qquad \Pi_2 = \frac{\widehat{S}_2}{R_N}, \tag{A.25}$$

one obtains

$$[\Pi_1, \Pi_2] = i\frac{\widehat{S}_3}{R_N^2}. \tag{A.26}$$

Since

$$S_3 = O(N), \qquad R_N^2 = O(N^2), \tag{A.27}$$

the coefficient behaves as

$$\frac{S_3}{R_N^2} = O(N^{-1}) \longrightarrow 0. \tag{A.28}$$

Keeping

$$J \equiv \widehat{S}_3 \tag{A.29}$$

as the rotation generator gives

$$[J, \Pi_1] = i\Pi_2, \qquad [J, \Pi_2] = -i\Pi_1, \qquad [\Pi_1, \Pi_2] = 0, \tag{A.30}$$

which is the ordinary $e(2)$ Inönü–Wigner contraction of $su(2)$.

The two large-N rescalings therefore have distinct meanings. The $1/\sqrt{N}$ scaling retains finite collective fluctuations and yields a non-trivial, centrally extended transverse algebra. The $1/R_N \sim 1/N$ scaling instead describes the geometrical contraction of the full collective representation: as the $SU(2)$ radius becomes macroscopically large, a local transverse region around the selected direction approaches a (tangent) plane, and the transverse generators become commuting translations.

Appendix B. The order parameter and collective modes in QFT

In quantum field theory, the $\psi(x_n)$ doublets are equal time anticommuting fields, $\{\psi_a(x_n), \psi_b^\dagger(x_m)\}_{t_n=t_m} = \delta_{a,b}\delta(\mathbf{x}_n - \mathbf{x}_m)$, $a, b = \pm$. The index n in x_n denotes different values of space $\mathbf{x}$ and times t; or different lattice sites $n = 1, 2, ..N...$ and times t in the case of a lattice, e.g., in the study of ferromagnets with localized $SU(2)$ spin

components [17, 20, 37]. All other anticommutators are equal to zero. The interaction among them is given in terms of a Lagrangian $L[\psi(x_n)]$ whose specific form does not need to be specified in our present discussion. We only assume that it is invariant under the $SU(2)$ transformations of the $\psi(x_n)$ fields in the $(\pm)$-space, $L[\psi(x_n)] = L[\psi^{'}(x_n)]$, with

$$\psi(x_n) \to \psi^{'}(x_n) = \exp(i\theta_i\lambda_i)\psi(x_n), \qquad i = 1, 2, 3, \tag{B.1}$$

where $\lambda_i = \sigma_i/2$ and θ_i denote the rotation angles in the $((+) - (-))$-space. The σ_i are the Pauli matrices

$$\sigma_1 = \begin{pmatrix} 0 & 1 \\ 1 & 0 \end{pmatrix}, \ \sigma_2 = \begin{pmatrix} 0 & -i \\ i & 0 \end{pmatrix}, \ \sigma_3 = \begin{pmatrix} 1 & 0 \\ 0 & -1 \end{pmatrix}. \tag{B.2}$$

Let $S^{(i)}(x_n), i = 1, 2, 3$, denote the generators of the $SU(2)$ algebra [20, 37],

$$[S^{(i)}(x_n), S^{(j)}(x_l)] = i\epsilon_{ijk}S^{(k)}(x_n)\delta_{n,l}. \tag{B.3}$$

In terms of the fields $\psi(x_n)$, their explicit expression is $S^{(i)}_{\psi}(x_n) = \psi^{\dagger}(x_n)(\sigma_i/2)\psi(x_n)$, with σ_i the Pauli matrices. The total $SU(2)$ generators are

$$S^{(i)} = \sum\nolimits_n S^{(i)}(x_n), \quad i = 1, 2, 3, \tag{B.4}$$

with the algebra

$$[S^{(i)}, S^{(j)}] = i\epsilon_{ijk}S^{(k)}. \tag{B.5}$$

$S^{(i)}(x_n)$ transforms as as

$$S^{(i)}(x_n) \to S^{(i)'}(x_n) = S^{(i)}(x_n) - \theta_j\epsilon_{ijk}S^{(k)}(x_n). \tag{B.6}$$

for θ_i infinitesimal.

Many *configurations* may be obtained by operating with the $SU(2)$ transformations on the individual doublets $\psi(x_n)$. We call them *microscopic configurations*. Those with the same value of the difference

$$\frac{1}{2}|(N_+ - N_-)| \equiv M \tag{B.7}$$

are considered to be equivalent.

M is called the polarization, or magnetization (as in the case of ferromagnets [17, 20, 37]). From the expression of $S^{(3)}$ in Eq. (B.4), it is not difficult to realize that $M = S^{(3)}$.

Although M has a microscopic origin, specified by Eq. (B.7), it behaves as a *macroscopic* variable characterizing the *macroscopic state* of the system, and it is called the "order parameter" field.

– Spontaneous breakdown of the symmetry and Collective modes

The ground state $|0\rangle$ characterized by zero magnetization $\langle 0|M|0\rangle = \mathcal{M} = 0$ is said to be the "normal" state, also denoted as $|0\rangle \equiv |0\rangle_{\mathcal{M}=0}$.

Spontaneous breakdown of the symmetry (SBS) is said to occur when [17, 20, 37], the ground state is not symmetric under $SU(2)$ transformations, although the dynamics described by the Lagrangian is assumed to be invariant under such transformations.

An external stimulus, due, e.g., to an information source, may produce SBS, i.e., a non-zero expectation value $\mathcal{M} \neq 0$ of the $S^{(3)}$ generator in the ground state:

$$\text{external stimulus} \;\rightarrow\; {}_{\mathcal{M}}\langle 0|S^{(3)}|0\rangle_{\mathcal{M}} \equiv \mathcal{M} \neq 0. \tag{B.8}$$

i.e., the stimulus induces the transition (SBS): $|0\rangle_{\mathcal{M}=0} \rightarrow |0\rangle_{\mathcal{M}\neq 0}$. Eq. (B.8) tells us that $|0\rangle_{\mathcal{M}}$ is not an SU(2) symmetric state.

Different values of $\mathcal{M}$ may be obtained as expectation values computed in different ground states, e.g., $|0\rangle_{\mathcal{M}}$, $|0\rangle_{\mathcal{M}'}$, with $\mathcal{M} \neq \mathcal{M}'$. These ground states can be shown to be each other orthogonal: ${}_{\mathcal{M}'}\langle 0|0\rangle_{\mathcal{M}} = 0$ in the large N limit, $\mathcal{M}' \neq \mathcal{M}$. We may refer to $\mathcal{M}$ as the "memory" of the information carried by the stimulus breaking the symmetry.

The meaning of the orthogonality ${}_{\mathcal{M}'}\langle 0|0\rangle_{\mathcal{M}} = 0$, for $\mathcal{M}' \neq \mathcal{M}$, in the large N limit, is that $|0\rangle_{\mathcal{M}'}$ cannot be expressed as a superposition of $|0\rangle_{\mathcal{M}}$ and states constructed from it (and vice versa), i.e., there is no unitary transformation connecting them in the large N limit. They belong to unitarily inequivalent state spaces.

Infinitely many unitarily inequivalent ground states (with their corresponding full state space, called representations of the canonical commutation or anticommutation relations) exist in QFT. In contrast, in quantum mechanics (QM), the von Neumann theorem forbids the existence of unitarily inequivalent ground states [17, 20, 30]. Therefore, we need the formalism of QFT.

Remarkably, the orthogonality ensures that there is no danger of memory "confusion" between any two different memories. Moreover, due to the said existence of infinitely many (unitarily inequivalent) orthogonal ground states, an enormous memory capacity is also guaranteed [21].

As said, the order parameter manifests itself as a macroscopic (classical) field. The "memory" of the stimulus encoded in $\mathcal{M}$ is thus described as a macroscopic property of the system, not of one of the many equivalent microscopic distributions of the $\pm$ individual fields (cf. Eqs. (B.7) and (B.8)). This does not happen in the sense of a "statistical average" over the microscopic distributions, but because SBS induces the dynamical formation of *collective modes* through the generation of long-range correlations among the elementary units, as shown by the Goldstone theorem. Its proof is not reported here for brevity (see [16–20]). We only recall that the functional integral formalism leads to the Ward-Takahashi identity

$$\langle S^{(3)}(x_m)\rangle_\epsilon = \epsilon \sum\nolimits_n \int dt \langle S^{(i)}(x_n) S^{(i)}(x_m)\rangle_\epsilon \;, \qquad i = 1, 2, \tag{B.9}$$

showing that $\langle S^{(3)}(x_m)\rangle_\epsilon$ is not zero in the $\epsilon \to 0$ limit (i.e., we have SBS with a non-zero expectation value for $S^{(3)}(x_m)$, cf. Eq. (B.8)) if and only if the two-point correlation function $\langle S^{(i)}(x_n)S^{(i)}(x_m)\rangle_\epsilon$ is associated with a zero-mass excitation, corresponding to a pole singularity. The ϵ term in the functional integral describes the input action as a transient (the $\epsilon \to 0$ limit). In other words, the symmetry breakdown triggered by the input is dynamically self-sustained, and therefore it is said "spontaneous".

The quanta associated with the 'transverse' $S^{(i)}S^{(i)}$-correlations, i=1,2, in Eq. (B.9), are the Nambu-Goldstone (NG) boson fields, which we denote as $B(x_n)$ and $B^\dagger(x_n)$. The pole singularity tells us that these fields are massless, i.e., they span the whole system, behaving indeed as long-range correlations, and, at zero momentum, they do not add energy to the ground state $|0\rangle_{\mathcal{M}}$. This is the statement of the Goldstone theorem.

The conclusion is that the basic fields $S^{(i)}(x_n)$, $i = \pm$ (or $i = 1, 2$), and $\psi(x_n)$ (or $S^{(3)}(x_n)$) manifest themselves to the observation as the $B(x_n)$, $B^\dagger(x_n)$, and the doublet field $\phi(x_n)$, respectively. They form an irreducible set of physical fields $\{\phi(x_n), B(x_n)\}$, annihilating the normal state: $B_{\mathbf{k}}|0\rangle = 0 = \phi_{\mathbf{k}}|0\rangle$, with $B_{\mathbf{k}}$ and $\phi_{\mathbf{k}}$ the annihilation operators for $B(x_n)$ and $\phi(x_n)$.

As a result of SBS, the $SU(2)$ transformations (B.6) (or (B.1)) for the basic fields $\psi(x_n)$ and $S^{(i)}(x_n)$ are *dynamically rearranged* [32, 37] into the group contraction $E(2)$. The transformations of the physical fields $B(x_n)$, $B^\dagger(x_n)$, and $\phi(x_n)$ are then:

$$\begin{aligned}
\phi(x_n) \to \phi^{'}(x_n) &= \phi(x_n) \\
B(x_n) \to B^{'}(x_n) &= B(x_n) + i\theta_1(\frac{M}{2})^{\frac{1}{2}} \\
B^\dagger(x_n) \to B^{'\dagger}(x_n) &= B^\dagger(x_n) - i\theta_1(\frac{M}{2})^{\frac{1}{2}}
\end{aligned} \tag{B.10}$$

for $\theta_2 = \theta_3 = 0$,

$$\begin{aligned}
\phi(x_n) \to \phi^{'}(x_n) &= \phi(x_n) \\
B(x_n) \to B^{'}(x_n) &= B(x_n) - \theta_2(\frac{M}{2})^{\frac{1}{2}} \\
B^\dagger(x_n) \to B^{'\dagger}(x_n) &= B^\dagger(x_n) - \theta_2(\frac{M}{2})^{\frac{1}{2}}
\end{aligned} \tag{B.11}$$

for $\theta_1 = \theta_3 = 0$, and

$$\begin{aligned}
\phi(x_n) \to \phi^{'}(x_n) &= e^{i\theta_3\lambda_3}\phi(x_n) \\
B(x_n) \to B^{'}(x_n) &= e^{-i\theta_3}B(x_n) \\
B^\dagger(x_n) \to B^{'\dagger}(x_n) &= e^{i\theta_3}B^\dagger(x_n)
\end{aligned} \tag{B.12}$$

for $\theta_1 = \theta_2 = 0$. It can be shown[37] that the $\phi(x_n)$, $B(x_n)$ and $B^\dagger(x_n)$ field equations are invariant under the transformations (B.10)-(B.12). Their generators are

$$S_f^{(1)} = (\frac{M}{2})^{\frac{1}{2}} \sum\nolimits_n [B(x_n) f(x_n) + B^\dagger(x_n) f^*(x_n)], \tag{B.13}$$

$$S_f^{(2)} = -i(\frac{M}{2})^{\frac{1}{2}} \sum\nolimits_n [B(x_n) f(x_n) - B^\dagger(x_n) f^*(x_n)], \tag{B.14}$$

$$S^{(3)} = \sum\nolimits_n [\phi^\dagger(x_n) \lambda_3 \phi(x_n) - B^\dagger(x_n) B(x_n)], \tag{B.15}$$

respectively. They close the $e(2)$ algebra (see Appendix A) and are time-independent ($f(x_n)$, introduced to make them mathematically well defined, is assumed to satisfy the field equation for B-modes. The limit $f(x_n) \to 1$ is taken after the generators have been operating.)

The translations for the field $B(x_n)$ and $B^\dagger(x_n)$ in Eqs. (B.10) and (B.11) generate their *coherent condensation* in the ground state [17, 39, 40] ($S_f^{(i)}$, $i = 1, 2$ in Eqs. (B.13) and (B.14) are in fact recognized to be generators of coherent states [37, 40]). 'Coherent' condensation means that correlation waves propagate without destructive interference. In the large N (infinite volume) limit ($f(x_n) \to 1$), these transformations cannot be induced by any unitary operator, which is consistent with the unitary inequivalence of the ground states (and the respective spaces) labeled by different values of $\mathcal{M}$.

In conclusion, as an effect of the action of the input, inducing SBS, we have $|0\rangle \to |0\rangle_{\mathcal{M}}$ and ${}_{\mathcal{M}}\langle 0|B^\dagger(x_n)B(x_n)|0\rangle_{\mathcal{M}} = \mathcal{M}$, for $\theta_2 = \theta_3 = 0$, and similar one for $\theta_1 = \theta_3 = 0$, showing that $\mathcal{M}$ provides a measure of the number of B-modes condensed in the ground state once the information carried by the input has been printed there. For $\theta_1 = \theta_2 = 0$, Eqs. (B.12) show that the ground state is invariant under rotations around the 3rd axis, in fact $\langle 0|B'^\dagger(x_n)B'(x_n)|0\rangle = 0$.

Summarizing, the $SU(2)$ generators $S^{(i)}(x_n)$, $i = 1, 2$ produce the flipping $+/-$ of the neural units $\psi(x_n)$. An input carrying information of code $\mathcal{M}$ induces SBS with the dynamical rearrangement of symmetry generating boson condensation (translation, shifts) of NG fields B and $B^\dagger$ (Eqs. (B.10) and (B.11)). These act as collective modes with long-range correlations among the component units, whose flipping by $SU(2)$ rotations around the axes 1 and/or 2 is now described in terms of coherent boson condensation (translation, shifts) of B and $B^\dagger$. The whole net thus acts as a single dynamical system. Memory states are thus collective, long-range, coherent modes, rather than "collections of data" describing the flippings of many (in principle, infinitely many for $N \to \infty$) local units.

More details and derivations, for brevity not reported here, can be found in the cited literature.

Appendix C. Dissipative Doubled Dynamics and the Finite-Lattice Response Functional

The purpose of this Appendix is to relate the doubled description of dissipative quantum field dynamics to the finite-lattice response quantity used in the Shift Test. The first part recalls the relevant QFT construction; the second introduces its finite-dimensional c-number counterpart. The correspondence is structural: the finite lattice does not reproduce the full quantum dissipative theory but retains the doubled physical/tilde organization and the corresponding algebraic contributions needed to construct a comparative response measure.

C.1 Doubled degrees of freedom in dissipative QFT

A canonical description of a dissipative open system can be obtained by embedding it into an enlarged system containing both the physical degrees of freedom and a corresponding tilde sector. In the dissipative QFT construction considered here, the Hamiltonian is

$$H = H_0 + H_I, \tag{C.1}$$

with

$$H_0 = \sum_\kappa \hbar\Omega_\kappa (A_\kappa^\dagger A_\kappa - \widetilde{A}_\kappa^\dagger \widetilde{A}_\kappa), \quad \text{and} \quad H_I = i\sum_\kappa \hbar\Gamma_\kappa (A_\kappa^\dagger \widetilde{A}_\kappa^\dagger - A_\kappa \widetilde{A}_\kappa). \tag{C.2}$$

Here A_κ denotes a boson mode of momentum k associated with the physical system and $\widetilde{A}_\kappa$ its doubled counterpart. The parameters Ω_κ and Γ_κ specify, respectively, the characteristic mode frequency and the coupling between the two sectors.

The first term measures the difference between the excitation contents of the physical and tilde sectors, whereas the second couples the two sectors and generates the dissipative evolution of the physical subsystem. Since

$$[H_0, H_I] = 0, \tag{C.3}$$

the difference $\mathcal{N}_{A_\kappa} - \mathcal{N}_{\widetilde{A}_\kappa}$ is conserved during the doubled evolution. H_0 is in fact proportional to the $SU(1,1)$ Casimir operator, and it is therefore invariant under the group transformations (cf. e.g., Eq. (C.3)). In the balanced sector relevant to the dissipative construction,

$$\mathcal{N}_{A_\kappa} = \mathcal{N}_{\widetilde{A}_\kappa}. \tag{C.4}$$

Once such a condition is assigned at the initial time t_0, it is conserved under time evolution. The doubling therefore provides a canonical representation in which the physical subsystem can exchange energy with its environment while the enlarged physical-plus-tilde system retains the conserved structure required by the formalism. The full $SU(1,1)$ coherent-state construction associated with this dynamics has been developed elsewhere [21, 41]; for the present purpose, Eqs. (C.1) - (C.4) provide the ingredients needed to establish the finite-lattice correspondence.

– From doubled operators to c-number amplitudes

The finite neural field evolves complex classical variables rather than creation and annihilation operators. We therefore consider the c-number counterpart of Eqs. (C2) and (C3). Replacing the operators by complex amplitudes,

$$A_\kappa \to A_\kappa^{(c)}, \qquad \widetilde{A}_\kappa \to \widetilde{A}_\kappa^{(c)}, \tag{C.5}$$

gives

$$A_\kappa^\dagger A_\kappa \longrightarrow \mid A_\kappa^{(c)} \mid^2, \qquad \widetilde{A}_\kappa^\dagger \widetilde{A}_\kappa \longrightarrow \mid \widetilde{A}_\kappa^{(c)} \mid^2 . \tag{C.6}$$

The first contribution therefore becomes

$$H_0^{(c)} = \sum_\kappa \hbar\Omega_\kappa (\mid A_\kappa^{(c)} \mid^2 - \mid \widetilde{A}_\kappa^{(c)} \mid^2). \tag{C.7}$$

For the interaction term, defining $z_\kappa = A_\kappa^{(c)} \widetilde{A}_\kappa^{(c)}$, one has $i(z_\kappa^* - z_\kappa) = 2\ Im z_\kappa$, and hence

$$H_I^{(c)} = 2 \sum_\kappa \hbar\Gamma_\kappa\ Im(A_\kappa^{(c)} \widetilde{A}_\kappa^{(c)}). \tag{C.8}$$

Thus the two algebraic structures $\mid A \mid^2 - \mid \widetilde{A} \mid^2$ and $2\ Im(A\widetilde{A})$ follow directly from the c-number realization of the doubled dissipative Hamiltonian.

– Finite-lattice realization

In the finite lattice, the corresponding amplitudes are constructed locally from the physical field ψ and the tilde field $\widetilde{\psi}$. Because the two sectors are represented in distinct dynamical frames, the tilde field is first transported into the physical frame before the two are combined.

To avoid confusion with the order parameter $\mathcal{M}$, we denote the corresponding transport map by

$$\mu : \widetilde{\psi} \longmapsto \mu\widetilde{\psi}. \tag{C.9}$$

For each lattice site n and internal component $\alpha = \pm$, we then define

$$A_{n\alpha} = \frac{1}{\sqrt{2}} \left[\psi_{n\alpha} + (\mu\widetilde{\psi})_{n\alpha} \right], \tag{C.10}$$

$$\widetilde{A}_{n\alpha} = \frac{1}{\sqrt{2}} \left[\psi_{n\alpha} - (\mu\widetilde{\psi})_{n\alpha} \right]. \tag{C.11}$$

These quantities should not be identified with the quantum operators A_κ and $\widetilde{A}_\kappa$. They provide their finite-dimensional c-number counterparts after the physical and tilde fields have been expressed in a common local frame. The symmetric component $A_{n\alpha}$ represents the locally aligned physical/tilde contribution, whereas $\widetilde{A}_{n\alpha}$ measures their antisymmetric mismatch.

Applying the correspondence of Eqs. (C.7) and(C.8) gives the finite-lattice quantities

$$H_0^p = \sum_{n,\alpha} \Omega_{n\alpha}(\mid A_{n\alpha} \mid^2 - \mid \widetilde{A}_{n\alpha} \mid^2), \tag{C.12}$$

$$H_I^p = 2 \sum_{n,\alpha} \Gamma_{n\alpha} Im(A_{n\alpha} \widetilde{A}_{n\alpha}). \tag{C.13}$$

The factor $\hbar$ has been absorbed into the effective finite-model scale. Eqs. (C.12) and (C.13) therefore preserve the algebraic form of the two contributions appearing in the doubled QFT Hamiltonian.

The transport map μ , by contrast, belongs specifically to the finite realization: it determines how the physical and tilde lattice fields are brought into correspondence before the doubled quantities are evaluated. It therefore provides the bridge between the doubled QFT structure and the finite variables used in the numerical model.

C.2 Doubled-field response functional

For the Shift Test we combine the two finite doubled contributions into the scalar functional

$$F^p = H_0^p + H_I^p. \tag{C.14}$$

The superscript p denotes the finite physical/tilde realization used in the numerical model. The quantity F^p is not the Hamiltonian generating the FIELD dynamics, nor is it identified with the physical energy of the neural field. Rather, it is a scalar response functional whose algebraic form is inherited from the doubled dissipative Hamiltonian and which allows different relaxed field configurations to be compared on a common basis.

In the Shift Test, the relevant quantity is its post-relaxation change relative to the corresponding unperturbed ordered state,

$$\Delta F^p = F^p_{relaxed,shift} - F^p_{relaxed,reference}. \tag{C.15}$$

The direct observables of the ordered field remain

$$\Delta S_3 \quad \text{and} \quad \Delta \mid \mathbf{S} \mid, \tag{C.16}$$

while ΔF^p provides an additional measure of the residual displacement of the doubled field configuration. A small value of $\mid \Delta F^p \mid$ indicates that, according to the doubled-field functional, the relaxed perturbed state remains close to its ordered reference; a larger value indicates a stronger residual displacement. Within the finite-lattice realization, F^p therefore plays the role of the model-level homologue of the energetic and dissipative balance represented by the doubled Hamiltonian. Correspondingly, ΔF^p provides a finite-model measure of the residual energetic-dynamical displacement produced by a perturbation after relaxation.

The Shift Test uses this measure together with ΔS_3 and $\Delta \mid \mathbf{S} \mid$ to determine whether perturbations transverse and longitudinal to the selected order direction produce dynamically distinct responses.

Appendix D. Transverse Long-Range Correlation and Spectral Analysis

D.1 Transverse field in the instantaneous order frame

At each time t , the local field state is represented by the three-component vector

$$\mathbf{s}(r,t) = (s_1,(r,t), s_2(r,t)s_3(r,t)), \tag{D.1}$$

and the instantaneous global order direction is obtained from

$$\mathbf{m}(t) = \frac{1}{N}\sum_r \mathbf{s}(r,t), \qquad \widehat{\mathbf{e}}_0(t) = \frac{\mathbf{m}(t)}{\mid \mathbf{m}(t) \mid}. \tag{D.2}$$

Two orthogonal unit vectors $\widehat{\mathbf{e}}_1$ and $\widehat{\mathbf{e}}_2$ are then chosen perpendicular to $\widehat{\mathbf{e}}_0$. The local transverse field is represented as the complex quantity

$$s_\perp(r,t) = \mathbf{s}(r,t) \ \cdot \ \widehat{\mathbf{e}}_1 + i \ \mathbf{s}(r,t) \ \cdot \ \widehat{\mathbf{e}}_2. \tag{D.3}$$

Thus, "transverse" is defined relative to the *instantaneous macroscopic order direction*, rather than to a permanently fixed coordinate axis. When the ordered state is predominantly aligned with S_3 , Eq. (C.2) reduces approximately to the familiar $s_1 + is_2$ representation.

The numerical implementation stores the unit-Bloch convention $\psi^\dagger\sigma_i\psi$. This overall factor does not affect the normalized spectral quantities reported below.

– *Long-range functional graph*

Spatial separation was measured using the toroidal Manhattan distance

$$d_T(i,j) = \min(\mid x_i - x_j \mid, L- \mid x_i - x_j \mid) + \min(\mid y_i - y_j \mid, L- \mid y_i - y_j \mid), \tag{D.4}$$

which accounts for the periodic lattice boundaries. Pairs with $d_T \geq 3$ were treated as long-range candidates.

For each candidate pair, the analysis computes a normalized similarity between the centered transverse components of the two sites. A *functional edge* is retained when this similarity increases relative to the immediately preceding frame,

$$w_{ij}(t) = \left[C_{ij}^{\perp}(t) - C_{ij}^{\perp}(t-\Delta t)\right]_+, \tag{D.5}$$

where $[x]_+ = \max(x,0)$. The edge weight therefore measures a newly increased transverse relation during the evolving trajectory. It does not represent a structural connection between sites.

For visualization, the participation of each site is summarized by its weighted degree,

$$k_i^{(w)} = \sum_j w_{ij}. \tag{D.6}$$

The functional graph in Figure 5 is used primarily as a spatial representation of the phenomenon. Because the number of possible pairs grows rapidly with lattice size, graph counts are not used as the principal finite-size evidence.

– Structure factor, low-k organization, and null models

The primary quantitative analysis therefore uses the transverse structure factor

$$S_\perp(\mathbf{k}) = \frac{1}{N} \mid \sum_r s_\perp(r)\ e^{-i\mathbf{k}\cdot r}\ \mid^2 . \tag{D.7}$$

This decomposes the transverse field according to spatial wavelength. Small non-zero $\mid \mathbf{k} \mid$ corresponds to slowly varying patterns extending over large portions of the lattice. We quantify this contribution by

$$f_{low\text{-}k} = \frac{\sum_{0<k^2\leq 2} S_\perp(\mathbf{k})}{\sum_{\mathbf{k}\neq 0} S_\perp(\mathbf{k})}. \tag{D.8}$$

The term *excess low-* $\mathbf{k}$ *organization* denotes the difference between this fraction in the empirical field and in a matched null model,

$$\Delta f_{low\text{-}k} = f_{low\text{-}k}^{emp} - \langle f_{low\text{-}k}^{null} \rangle. \tag{D.9}$$

A positive value therefore means that the actual transverse field contains *more spatially extended structure than expected after destroying its spatial organization while retaining relevant local properties.*

Two null models were used. The *null spatial-shuffle* randomly permutes the complex transverse values among lattice sites, preserving the set of local field values while destroying their spatial arrangement. The *null phase-randomized* preserves $\mid s_\perp(r) \mid$ at each site while replacing its phase by a random value. Three independent realizations of each null were generated for every empirical frame.

D.2 Radial correlation, simulation protocol, and controls

As a complementary test, we calculated the connected transverse correlation function

$$C_\perp^{conn}(d) = \left\langle Re\left[\delta s_\perp(r)\delta s_\perp^*(r')\right]\right\rangle_{d_T(r,r')=d}, \tag{D.10}$$

where

$$\delta s_\perp(r) = s_\perp(r) - \langle s_\perp \rangle. \tag{D.11}$$

This quantity relates to whether transverse deviations at pairs of sites separated by distance d remain correlated after removal of the spatial mean. The periodic correlation was evaluated by Fourier autocorrelation and then averaged over pairs having the same toroidal Manhattan distance. Its long-distance tail was examined for $d \geq \lceil L/4 \rceil$. Unlike the low-k measure, this radial statistic did not show a robust excess over the null models.

The reference analysis used $L = 8,\ 12,\ 16,\ 20\ , 32$ paired random seeds (42–73), and both correct and permuted branches. A source perturbation of strength 3.0 was applied for 24 steps to establish S_3 -dominated order. It was followed by three structured action pulses, each lasting eight steps, yielding 24 action frames per trajectory. In the correct branch, the sequence was pulse_x $\rightarrow$ pulse_y $\rightarrow$ pulse_diag ; in the permuted control, its order was reversed. The same initial condition and dynamical parameters were used for the paired branches.

For statistical comparisons, the three null realizations were first averaged within each lattice size, seed, and branch. The empirical-minus-null difference was then calculated for each seed, so that the seed - not the individual frame - served as the independent replication unit. The reported 95% confidence intervals were calculated from these paired seed-level differences. For the pooled result across lattice sizes, the four L values were first averaged within each seed before calculating the group statistics.

Finally, a transport control set the spatial transport coefficient to zero while increasing the source drive so that macroscopic longitudinal order remained at least as strong as in the reference condition. The disappearance of a consistent low-k excess under this control separates large-scale transverse organization from the mere presence of strong S_3 polarization.

References

[1] Freeman WJ (1975) Mass action in the nervous system. Academic Press, New York

[2] Freeman WJ (2000) Neurodynamics: An exploration of mesoscopic brain dynamics. Springer, Berlin

[3] Skarda CA, Freeman WJ (1987) How brains make chaos in order to make sense of the world. Behavioral and Brain Sciences 10:161-195

[4] Freeman WJ (1991) The physiology of perception. Scientific American 264:78-85

[5] Freeman WJ (2007) Intentionality. Scholarpedia 2(2):1337 www.scholarpedia.org/article/Intentionality. Accessed 28 September 2026

[6] Kozma R, Freeman WJ (2026) Cognitive phase transitions in the cerebral cortex – Enhancing the neuron doctrine by modeling neural fields (Second Edition). Springer, Heidelberg

[7] Freeman WJ, Quian Quiroga R (2013) Imaging brain function with EEG. Springer Science, New York

[8] Freeman WJ, Vitiello G (2006) Nonlinear brain dynamics as macroscopic manifestation of underlying many-body dynamics. Phys. of Life Reviews 3:93 – 117

[9] Freeman WJ, Vitiello G (2016) Matter and mind are entangled in two streams of images guiding behavior and informing the subject through awareness. Mind and Matter 14:7-24.

[10] Ricciardi LM, Umezawa H (1967) Brain physics and many-body problems. Kibernetik 4:44–48. Reprinted in: Globus GG, Pribram KH, Vitiello G (eds) (2004) Brain and Being. John Benjamins, Amsterdam, pp. 255 – 266

[11] Stuart CIJ, Takahashi Y, Umezawa H (1978) On the stability and non-local properties of memory. J. Theor. Biol. 71:605–618

[12] Stuart CIJ, Takahashi Y, Umezawa H (1979) Mixed system brain dynamics: neural memory as a macroscopic ordered state. Found. Phys., 9:301-327

[13] Sivakami S, Srinivasan V (1983) A model for memory. J. Theor. Biol. 102:287–294

[14] Jibu M, Yasue K (1995) Quantum brain dynamics and consciousness. John Benjamins, Amsterdam

[15] Jibu M, Pribram KH, Yasue K (1996) From conscious experience to memory storage and retrieval: the role of quantum brain dynamics and boson condensation of evanescent photons. Int. J. Mod. Phys. B10:1735–1754

[16] Itzykson C, Zuber J (1980) Quantum Field Theory. McGraw-Hill Inc., New York

[17] Umezawa H, Matsumoto H, Tachiki M (1982) Thermo Field Dynamics and Condensed States. North-Holland, Amsterdam

[18] Umezawa H (1993) Advanced field theory: micro, macro and thermal concepts. American Institute of Physics, New York

[19] Anderson PW(1984) Basic Notions of Condensed Matter Physics. Addison-Wesley, New York

[20] Blasone M, Jizba P, Vitiello G (2011) Quantum Field Theory and its macroscopic manifestations. Imperial College Press, London

[21] Vitiello G (1995) Dissipation and memory capacity in the quantum brain model. Int. J. Mod. Phys. B9:973–989

[22] Vitiello G (2001) My Double unveiled. John Benjamins, Amsterdam

[23] Vitiello G (2004) The dissipative brain. In: Globus GG, Pribram KH, Vitiello G (eds) (2004) Brain and Being. John Benjamins, Amsterdam, pp. 315–334

[24] Capolupo A, Freeman WJ, Vitiello G (2013) Dissipation of dark energy by cortex in knowledge retrieval. Physics of Life Reviews 10 (1):85-94

[25] Atmanspacher H (2024) Quantum approaches to consciousness. In: Zalta EN (ed) Stanford Encyclopedia of Philosophy. http://plato.stanford.edu/entries/qt-consciousness/ Accessed 28 September 2026

[26] Pessa E, Vitiello G (1999) Quantum dissipation and Neural Net Dynamics. Bioelectrochem and Bioenergetics 48:339–342

[27] Pessa E, Vitiello G (2003) Quantum noise, entanglement and chaos in the quantum field theory of mind/brain states. Mind and Matter 1:59–79

[28] Pessa E, Vitiello G (2004) Quantum noise induced entanglement and chaos in the dissipative quantum model of brain. Int. J. Mod. Phys. B18:841–858

[29] Basti G, Capolupo A, Vitiello G (2017) Quantum field theory and coalgebraic logic in theoretical computer science. Progr. Biophys. Mol. Biol. A130:39–52

[30] von Neumann J (1958) The computer and the brain. Yale University Press, New Haven

[31] Inönü E, Wigner EP (1953) On the contraction of groups and their representations. Proc. Nat. Acad. Sci. US 39:510–524

[32] De Concini C, Vitiello G (1976) Spontaneous breakdown of symmetry and group contraction. Nuc. Phys. B116:141–156

[33] Terenzi G (2026) From completion to composition in a finite-lattice field neural network, in preparation

[34] Terenzi G (2026) Making field-theoretic neural models observable: A mesoscopic observation bridge to MEA recordings, in preparation

[35] Beige A, Night PL, Vitiello G (2005) Cooling many particles at once, New J. of Physics 7:96

[36] Holstein T, Primakoff H (1940) Field Dependence of the Intrinsic Domain Magnetization of a Ferromagnet. Phys. Rev. 58:1098–1113

[37] Shah MN, Umezawa H, Vitiello G (1974) Relation among spin operators and magnons. Phys. Rev. B10:4724–4726

[38] De Concini C, Vitiello G (1977) Relation between projective geometry and group contraction in spontaneously broken symmetry theories. Phys. Lett. 70B:355–357

[39] Klauder JR, Sudarshan EC (1968) Fundamentals of quantum optics. Benjamin, New York

[40] Perelomov A (1986) Generalized coherent states and their applications. Springer-Verlag, Berlin

[41] Celeghini E, Rasetti M, Vitiello G (1992) Quantum dissipation. Annals of Physics (N.Y.) 215:156–170